

M Ű E G Y E T E M 1 7 8 2

**CHARACTERIZATION OF THE NUMERICAL DAMPING IN
THE MODAL ANALYSIS OF FORCED PIECEWISE LINEAR
ELASTIC STRUCTURES**

Budapest University of Technology and Economics

Faculty of Civil Engineering

Department of Structural Mechanics

THESIS BOOKLET

Bilal Alzubaidi

Supervisor: Dr. Róbert K. Németh

November 14, 2025

1 Introduction

A specific group of nonlinear systems that can be found in nature is the piecewise linear elastic systems. Piecewise linear elastic systems are those systems whose stiffness experiences a piecewise constant nature during vibration, depending on their displacements at a certain time instant. Inside the range where the stiffness is constant, the behavior is linear elastic. So, piecewise linear elasticity also means that as long as the structure maintains the same state of stiffness, i.e., over the same linear segment of its stress-deformation relationship, the linearity allows the application of modal analysis. Thus, the analysis of a multi-degree-of-freedom (MDOF) system simplifies to that of single-degree-of-freedom (SDOF) systems. While the vibration modes behave as independent linear oscillators, their combination, i.e. the original MDOF system, must be checked for a state switching condition in each time step. Every time a switch occurs, the modal displacements and velocities must be calculated in the new state from those of the previous state so that the physical shape and velocity match.

Sources of piecewise linearity in nature can be the slackening of a tensioned cable and the closure of an open gap. Both examples were considered in the dissertation.

2 The analyzed piecewise linear elastic structures: mechanical models and modal parameters

2.1 Discrete bar in tension and compression

The first piecewise linear elastic system introduced is a discrete bar in tension and compression subjected to unilateral contact. This model represents a multi-story building with potential contact at one of its floor levels with a neighboring structure, as can be seen in Fig 1. The source of piecewise linearity arises from the system having different stiffnesses pre- and post-contact, resulting in a different number of DOFs and a distinct equation of motion for each vibration state, which in turn produces different mode shapes and natural circular frequencies. The closure of the gap between the structure and the rigid wall is assumed to be fully plastic, which means that the roof level loses its velocity at the time instant of the impact. The energy loss caused by the plastic impact can represent one of the nonlinearities in buildings where we have clearances, such as in cracked reinforced concrete elements or in bolted steel connections. The change in the stiffness caused by the closure of these clearances in buildings is unable to bounce the whole building back under dynamic loading, so the resulting building stiffness change lasts for some time until the bending stiffness of the main stiffening elements restores the global displacements. This is the main reason behind the introduction of the perfectly plastic impact.

Since the vibration in each state exhibits linear elastic characteristics, modal analysis was employed to formulate the response function of the structure during a given state. Switching formulae from one state to another were subsequently derived under the assumption that, at the moment of a state transition, the impacting mass completely loses its kinetic energy, while the displacements and velocities of the rest of the structure remain unchanged.

This case is equivalent to the harmonically forced discrete MDOF system shown in Fig. 1a)-c), where each DOF has a mass m , representing the mass of the slabs, beams and column at each level, and each spring has a stiffness k , representing the lateral stiffness

produced by these building elements. At the boundaries, the system is constrained against horizontal displacement on one end, and subjected to a unilateral contact surface on the other end using the Signorini conditions, representing the rigid wall next to the building.

This assumption divides the motion into two linear states of stiffness. The first state is the sticking state, herein after called *state I*, where the last mass is stuck to the wall as in 1b), has a number of masses contributing in the equation of motion denoted by N^I . The second state is the free-flight state, herein after called *state II*, where the structure is free of contact, as in 1c), has a number of masses contributing in the equation of motion denoted by $N^{II} = N^I + 1$. During the vibration, the impact of the N^{II} -th mass on the wall is assumed to be perfectly plastic, i.e. the coefficient of restitution is equal to zero. In the current analysis, there is no prestressing in the model; the unloaded state of the system can be considered to belong to both of them, i.e. the mass is in touch with the wall but exerts no force on it.

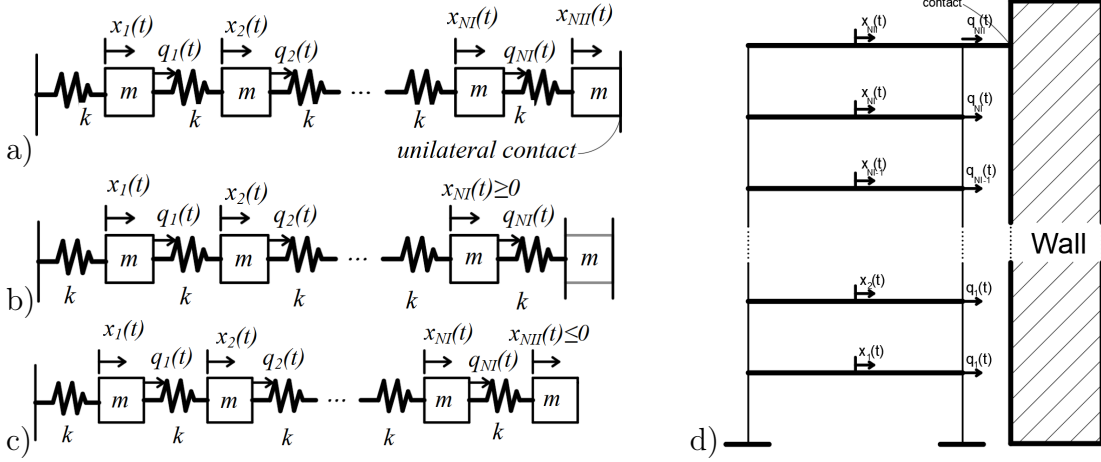


Figure 1: The piecewise linear elastic structure: a) system at equilibrium, b) system in state *I*, c) system in state *II*, and d) multi-storey PL structure

Under harmonic excitation, the matrix differential equation of motion in state α , where α can be *I* or *II*, is:

$$\mathbf{M}^\alpha \ddot{\mathbf{x}}^\alpha(t) + \mathbf{K}^\alpha \mathbf{x}^\alpha(t) = \mathbf{q}_0^\alpha \cos(\omega t - \phi). \quad (1)$$

In the above equation, \mathbf{M}^α and \mathbf{K}^α are the mass and stiffness matrices in state α , $\mathbf{x}^\alpha(t)$, $\ddot{\mathbf{x}}^\alpha(t)$ and \mathbf{q}_0^α are the vectors of displacements, accelerations and forcing amplitudes, respectively, that belong to state α and have a size of N^α -by-1. The symbol (\cdot) represents derivation with respect to time. The symbols ω and ϕ are the forcing frequency and its phase angle, respectively. The natural circular frequencies and the mode shapes in both states are the result of the generalized eigenvalue problem. The solutions of the differential equations of motion in Eq. (1) were performed using *modal analysis*. The displacement of the structure in state α is written as a linear combination of the eigenvectors:

$$\mathbf{x}^\alpha(t) = \mathbf{V}^\alpha \boldsymbol{\eta}^\alpha(t), \quad (2)$$

where \mathbf{V}^α is the N^α -by- N^α modal matrix of the mass matrix normalized eigenvectors and $\boldsymbol{\eta}^\alpha(t)$ is the vector of modal displacements.

At certain time instants during the vibration, the system changes its state depending on the conditions around the boundary and its interaction with the contact surface. The unilateral contact can be formulated as the one-dimensional form of the Signorini conditions.

The system remains in state I as long as there is a compressive reaction force from the contact surface, and the sign of the reaction force can be obtained from the spring force in the spring connecting the mass in contact, which is only affected by the displacement of them. Thus, the condition on the reaction force can be represented by the following inequality:

$$\mathbf{h}^{I\top} \mathbf{x}^I \geq 0. \quad (3)$$

The vector \mathbf{h}^I is the N^I -th unit vector, making sure that the force in the last spring will be in compression in order to maintain a positive reaction force. Similarly, the system remains in state II as long as there is a gap between the contact surfaces. Generally, this can be represented by the following inequality:

$$\mathbf{h}^{II\top} \mathbf{x}^{II} \geq 0. \quad (4)$$

The vector \mathbf{h}^{II} is the opposite of the N^{II} -th unit vector, making sure that the last DOF does not penetrate the wall. Here, we note that Eqs.(3)-(4) are not used to decide the current state of the motion, only to check if the system remains in the currently assumed state. Specifically, in state II the constraint of Eq.(4) must be true, but Eq.(3) is irrelevant until the switch from state II to I , the $\mathbf{h}^{I\top} \mathbf{x}^I$ product, even if only formally, could be negative, as well.

This system was further analyzed in Chapter 4, where a modal analysis-based method was demonstrated to obtain the periodic paths and vibrations of the system. In Chapter 5, the energy loss due to the impact was characterized using a single viscous damping ratio.

2.2 Continuum beam supported by block-and-tackle suspension system

The second system analyzed in this dissertation is a beam continuously supported by block-and-tackle suspension system. This type of suspension offers a way of supporting structural elements in multiple points with a slight increase in the static indeterminacy. In this constraint, a cable is driven through pulleys placed at certain points along the beam length, as shown in Fig 2a) and b). The aim here is to analyze the special (theoretical) case of a simply-supported beam where it is supported by a cable and the pulleys are continuously placed along a certain segment of the beam, which can be seen in Fig. 2c).

The source of the piecewise linearity in our beam is that under any displacement, the cable is either slacked or tensioned, which divides the motion into 2 PL states. In case of a slacked cable, the beam is said to be in the *passive state*, while in case of a tensioned cable, the beam is said to be in the *active state*. It is to note here that the current analysis is restricted to a special case of this structure where the integral of the suspended points' displacements is equal to zero. This case can also happen if the beam is supported by a double cable, i.e. a cable from top and a cable from bottom, then the beam is considered to be always in the *active state* and the integral of the suspended points' displacement will always be zero. The parameters, namely the natural circular frequencies, vibration shapes, critical forces and buckling shapes, are affected by the continuous suspension. In this section, only the method of the solution derivation of the dynamic and static differential equations is shown, exploiting the boundary and continuity conditions introduced by the beam ends and the cable, respectively. The analyses of the effect of the continuous cable support on the free vibration and buckling of the beam are left to the next chapter.

The analyzed beam in Fig. 2c) is an Euler-Bernoulli beam of length L , bending stiffness EI , mass density ρ and specific mass μ . The principal displacement is denoted

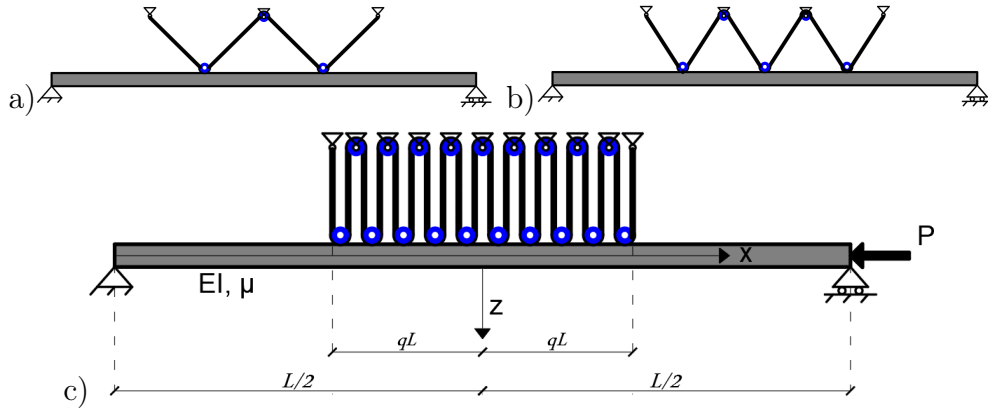


Figure 2: Mechanical model of the continuum beam suspended by block-and-tackle system at a) 2 points, b) 3 points, and c) an infinite number of points.

by $w(x)$, which is the displacement of the beam axis in the z -direction. The beam is simply-supported; it has a pinned joint on the left end and a roller on the right end.

In the *passive state*, the presence of the cable is neglected, and the problem is a classical Euler-Bernoulli beam. In the *active state*, due to the tension force in the cable, the beam is divided into three segments, with $w_1(x)$, $w_2(x)$ and $w_3(x)$ being their displacements, and they are assumed to be harmonic. The beam is continuously supported on segment 2, while segments 1 and 3 are unsupported. The cable is assumed to be of infinite normal stiffness and supports segment 2 by infinitely many points and exerts an S_0 continuously distributed load on the beam. The supported length of the cable extends a qL distance from the origin equally in both directions, making $2qL$ as the total supported length.

After the substitution of the assumed solutions, $w_1(x)$, $w_2(x)$ and $w_3(x)$, into the differential equations of an Euler-Bernoulli beam for each segment, it yields:

$$EI \frac{d^4 w_1(x)}{dx^4} - \mu \omega_0^2 w_1(x) = 0, \quad (5)$$

$$EI \frac{d^4 w_2(x)}{dx^4} - \mu \omega_0^2 w_2(x) - S_0 = 0, \quad (6)$$

$$EI \frac{d^4 w_3(x)}{dx^4} - \mu \omega_0^2 w_3(x) = 0. \quad (7)$$

For the buckling analysis, the static ordinary differential equations for the three segments are:

$$EI \frac{d^4 w_1(x)}{dx^4} + P \frac{d^2 w_1(x)}{dx^2} = 0, \quad (8)$$

$$EI \frac{d^4 w_2(x)}{dx^4} + P \frac{d^2 w_2(x)}{dx^2} - S_0 = 0, \quad (9)$$

$$EI \frac{d^4 w_3(x)}{dx^4} + P \frac{d^2 w_3(x)}{dx^2} = 0. \quad (10)$$

The general solutions of the homogeneous differential equations contain 4–4 parameters, while the solutions of the non-homogeneous differential equations have 4–4 parameters from the general solution of the complementary homogeneous equation and one parameter from the particular solution. In each case, there are a total of 13 parameters that must be related to each other such that they fulfill the following 13 constraints:

- at each end of the beam, the displacements and moments are zero (4)

- at the conjunction of segments 1 and 2, the displacements, rotations, moments and shears are continuous (4)
- at the conjunction of segments 2 and 3, the displacements, rotations, moments and shears are continuous (4)
- the integral of the displacements in segment 2 equals zero (1)

These constraints are used to form the frequency matrix and the buckling matrix, which will be presented in the next chapter.

3 The effect of continuous suspension constraint on the free vibration and buckling of a beam

In this chapter, the aim was to analyze the effect of the continuous support on the buckling and the free vibration properties of the beam. As the suspension cable is attached to the simply-supported beam, it affects the natural circular frequencies, the critical forces, the vibration modes, and the buckling modes. This effect is analyzed as a function of the length of the suspended segment. The natural circular frequencies or the critical forces of the beam are calculated as a function of the length of the continuous support and presented in a frequency map or a buckling map, respectively.

First, the derivation of the frequency and buckling matrices of this beam is shown, the determinant is drawn versus the frequency or the buckling parameters, the zero points of the determinants are stored, and the frequency and buckling maps are calculated for the first 9 modes alongside the mode shapes. Finally, a generic example of the suspended beam is used to validate the results against a discretized solution using the Finite Element Method (FEM).

As mentioned earlier, the presence of the cable divides the stiffness of the beam into 2 PL elastic states. In the passive state, the cable is slackened, and the beam behaves as a classical simply-supported beam. So, the solution of the beam in the passive state will be omitted here.

3.1 Dynamic analysis in the active state

In the active state of the beam, the general solutions of the dynamic problem are:

$$w_1(x) = A_1 \sin(\lambda x) + A_2 \cos(\lambda x) + A_3 \sinh(\lambda x) + A_4 \cosh(\lambda x), \quad (11)$$

$$w_2(x) = A_5 \sin(\lambda x) + A_6 \cos(\lambda x) + A_7 \sinh(\lambda x) + A_8 \cosh(\lambda x) - \frac{S_0}{\mu \lambda^4}, \quad (12)$$

$$w_3(x) = A_9 \sin(\lambda x) + A_{10} \cos(\lambda x) + A_{11} \sinh(\lambda x) + A_{12} \cosh(\lambda x). \quad (13)$$

Here, λ is the frequency parameter. These solutions are substituted in the 13 boundary conditions from the previous chapter. This substitution yields a system of linear equations in the form:

$$\mathbf{F}_a \mathbf{a}_a = 0, \quad (14)$$

where the vector \mathbf{a}_a contains the unknown parameters with a size of 13x1 and \mathbf{F}_a is the frequency matrix built from the coefficients of the parameters with a size of 13x13.

The solutions of Eq. (14) are obtained when the determinant of $\mathbf{F}_a = 0$. The matrix \mathbf{F}_a depends on two parameters: q and λ . The non-trivial solution points of Eq. (14) can be shown as curves in the $q - \lambda$ plane. These curves are referred to as the frequency

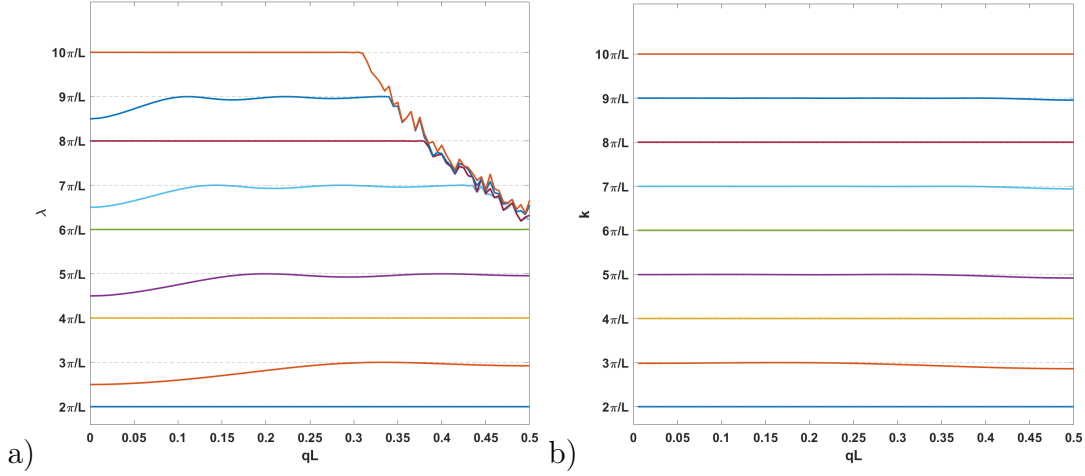


Figure 3: a)Frequency and b)buckling maps of the analyzed beam.

map. Here, it is shown only for the first 9 modes in Fig. 3a) Two observations can be noticed from Fig. 3a): first is that on the top right corner, there exists a disturbance of the solution lines due to the instability of the determinant at these λ values. Thus, it was hard to detect the exact zero value of the determinant of \mathbf{F}_a matrix. These solutions at this region are called parasitic solutions. The second observation is that the odd modes are horizontal straight lines, so they are not affected by the presence of the cable. On the contrary, the even modes are curved and have a maximum λ of

$$\lambda_{2j}^{max} = (2j + 1)\pi \quad (15)$$

value and it reaches the λ_{2j}^{max} value exactly at j values of q , namely at the

$$q_j^l = \frac{l}{2j + 1}, \quad l = 1, 2, \dots, j \quad (16)$$

points.

3.2 Buckling analysis in the active state

A similar procedure is carried out for the buckling analysis. In the active state of the beam, the general solutions are:

$$w_1(x) = B_1 \sin(kx) + B_2 \cos(kx) + B_3x + B_4, \quad (17)$$

$$w_2(x) = B_5 \sin(kx) + B_6 \cos(kx) + B_7x + B_8 + \frac{S_0x^2}{2EI k^2}, \quad (18)$$

$$w_3(x) = B_9 \sin(kx) + B_{10} \cos(kx) + B_{11}x + B_{12}. \quad (19)$$

Here, k is the buckling force parameter. These solutions are substituted in the 13 boundary conditions from the previous chapter. This substitution yields a system of differential equations in the form:

$$\mathbf{S}_a \mathbf{b}_a = 0, \quad (20)$$

where the vector \mathbf{b}_a contains the unknown parameters with a size of 13x1 and \mathbf{S}_a is the buckling matrix built from the coefficients of the parameters with a size of 13x13.

The nontrivial solutions of Eq. (20) are obtained when the determinant of $\mathbf{S}_a = 0$. The matrix \mathbf{S}_a depends on two parameters: q and k . The non-trivial solution points of Eq. (20) can be shown as curves in the $q - k$ plane. These curves are referred to as

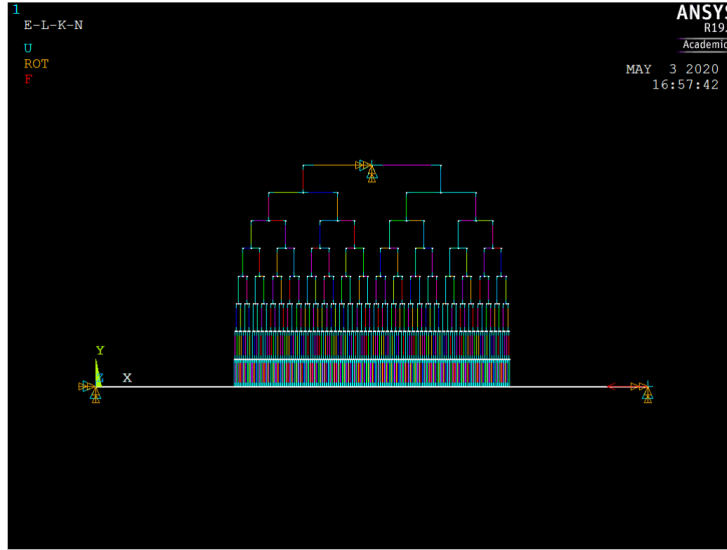


Figure 4: Samples of the FE models built for the convergence analysis with 256 beam elements, respectively.

the buckling map. Here, it is shown only for the first 9 modes in Fig. 3b) Similar to the frequency map, it can be observed from Fig. 3b) that the lines representing the odd modes are horizontal straight lines, which means that the odd modes are not affected by the presence of the cable. On the contrary, the even modes are curved lines of the j -th even mode never exceeds

$$k_{2j}^{max} = (2j + 1)\pi \quad (21)$$

value and it reaches the k_{2j}^{max} value at exactly j values of q , namely at

$$q_j^l = \frac{l}{2j + 1}, \quad l = 1, 2, \dots, j \quad (22)$$

points. It is to note that the buckling map does not contain parasitic solutions; the determinant had a clean, stable behavior due to the absence of the hyperbolic functions in the general solution equations.

3.3 Validation against a FE model

To validate the semi-analytical results, the calculated natural circular frequencies and critical loads were compared to those calculated in the commercial finite element software ANSYS for a member of the analyzed family with $q = 0.25$. As the continuous constraint is not presented in the software, it was substituted with a swing system, which allows obtaining the sum of the displacements of multiple points of the constraint, while the transmitted internal reaction forces are the same. The latter is the reason why swing systems are used in experiments to simulate distributed loads. Convergence analyses have been performed on the number of beam elements and stiffness of the bars of the swing system. The swing system, which can be seen in Fig. 4, is the converged version, where the beam is modelled with 256 beam elements.

As an example, the following material parameters and geometry were employed in the ANSYS model. A square cross-section with a side length of 2 cm was selected as the preferred design. Area and inertia were thus 4 cm^2 and $1.333 \times 10^{-8} \text{ m}^4$, respectively. A bending stiffness of 13.33 Nm^2 was obtained by using a Young's modulus of 10^9 N/m^2 . A specific mass of 0.8 kg/m was obtained from the mass density of 2000 kg/m^3 . The beam is 1 m in length.

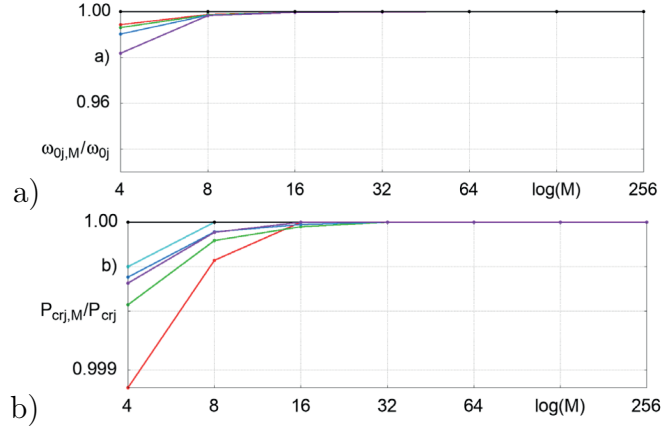


Figure 5: Convergence with the number of discrete suspension points of a) the ratios of the natural circular frequencies, and b) the ratios of the critical forces

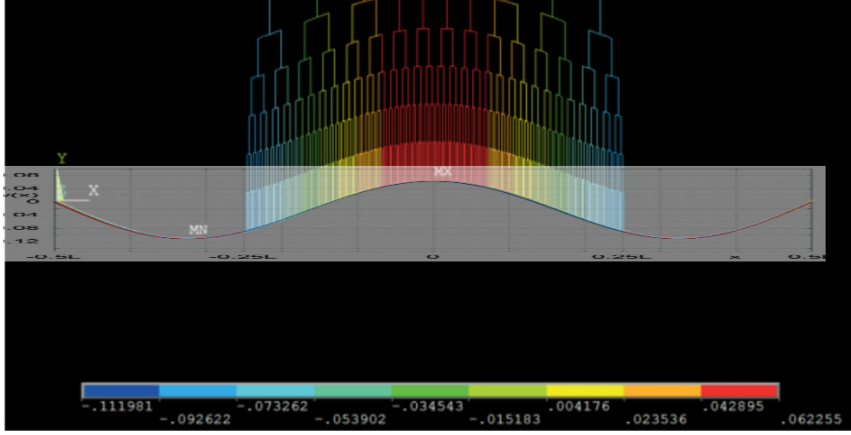


Figure 6: The second vibration mode of the beam with $q = 0.25$ of the semi-analytical and numerical methods combined.

To compare the results of the semi-analytical approach to the FEM, Fig. 5 shows the convergence analysis done for the FE model with the ratio of obtained natural circular frequencies and the buckling forces from both methods against the number of suspension points.

Lastly, a comparison was performed between the second vibration shape of the two methods. Figure 6 shows that the mode shapes are close to each other; both mode shapes share the same maximum (0.0622) and minimum (-0.111) values, and the curves are almost identical.

4 Modal analysis-based calculation of periodic paths and responses of harmonically forced piecewise linear elastic structures

In this chapter, the aim is to present a new method for the calculation of the periodic paths and responses of harmonically forced PL elastic MDOF structures, an example of them is the one shown in Fig. 1. The two states of the systems are such that the equilibrium position of the structure is on the switching surface, i.e., a switch between the states may occur there. Here, the vibrations that are of interest go through exactly one switch in each direction during a period of forcing. For the high number of DOFs, the advantages

of modal analysis are used in obtaining the response of the linear elastic segments. It is worth mentioning that the method can also be extended to capture vibrations that undergo multiple impacts per period.

4.1 The method for obtaining periodic responses

In the proposed method, the time spent in the two states (T^I , T^{II}) alongside the forcing phase angle ϕ are treated as parameters. To get those vibrations that include exactly one switch in each vibration period $T = T^I + T^{II}$, the initial modal phase vector should satisfy the periodicity condition: $\hat{\boldsymbol{\eta}}^I(0) = \hat{\boldsymbol{\eta}}^I(T)$. For this, the system's modal phase vector should be calculated at the end of state I (at $t = T^I$, i.e. $\hat{\boldsymbol{\eta}}^I(T^I)$), switched to state II at $t = T^I$ ($\hat{\boldsymbol{\eta}}^{II}(T^I)$), calculated at the end of the state II ($\hat{\boldsymbol{\eta}}^{II}(T)$), and switched back to state I ($\hat{\boldsymbol{\eta}}^I(T)$). The consecutive substitution of these equations into each other will result in the following system of linear equations:

$$\mathbf{D}\hat{\boldsymbol{\eta}}^I(0) = \mathbf{d}. \quad (23)$$

The solution of Eq. (23) yields, for any (T^I, T^{II}, ϕ) triplet, those *periodic initial conditions* which result in a periodic response as long as the desired and only the desired switches occur at their respective times.

With the periodic initial conditions, it must also be ensured that the switches occur at the correct times, which means that the following two families of conditions must be met: (1) at the $t = T^I$ and at the $t = T$ time instances, the switch *must* occur, and (2) no switch may occur in the $0 < t < T^I$ and the $T^I < t < T$ intervals, i.e. the system *remains* in the current state. For the first conditions, two error functions are formulated to check the switching conditions:

$$f^I(T^I, T^{II}, \phi) = \mathbf{g}^{IT} \boldsymbol{\eta}^I(T^I) - \mathbf{q}_r^{II}, \quad f^{II}(T^I, T^{II}, \phi) = \mathbf{g}^{IIT} \boldsymbol{\eta}^{II}(T). \quad (24)$$

These error functions should be zero at those parameter values where the initial conditions result in a periodic vibration that fulfills the switching conditions. Solution of the system of nonlinear equations:

$$f^I(T^I, T^{II}, \phi) = 0, \quad f^{II}(T^I, T^{II}, \phi) = 0 \quad (25)$$

yields typically a one-dimensional manifold in the parameter space. To obtain the points of this manifold, a selected domain of the $T^I - T^{II} - \phi$ space is scanned, which is referred to as the Global Representation Space (GRS). The Scanning Simplex Algorithm introduced in Gáspár, Domokos, and Szeberényi 1997 is used for scanning.

The final step of the computation serves to filter out those solutions where a premature switch occurs in either case. For every (T^I, T^{II}, ϕ) triplet resulting from the scanning, the periodic initial conditions have to be calculated with the formulation and the solution of Eq. (23).

Then, a time-history calculation must be done with the obtained initial conditions, while the constraint corresponding to staying in the current state must be checked in every time step. If the first remaining condition holds for every t_i time steps in the $0 < t_i < T^I$ time interval, i.e. the system remains in state I :

$$\mathbf{g}^{IT} \boldsymbol{\eta}^I - \mathbf{q}_r^{II} \geq 0, \quad (26)$$

and after the switching, the second remaining condition holds for every t_i time step in the $T^I < t_i < T$ time interval, i.e. the system remains in state II :

$$\mathbf{g}^{IIT} \boldsymbol{\eta}^{II} \geq 0, \quad (27)$$

then the given solution can be referred to as a periodic response of the selected problem.

4.2 Examples: Periodic paths and responses of the PL elastic structure

The analyzed structure is the one in Fig. 1a), with forcing vectors:

$$\mathbf{q}^I = [1 \ 1 \ \dots \ 1]^\top, \quad \mathbf{q}^{II} = [1 \ 1 \ \dots \ 1 \ 1]^\top. \quad (28)$$

As a first example, the system analyzed contained 3 DOFs in state II , and referred to as $N23$.

The 3-dimensional parameter space of T^I - T^{II} - ϕ was scanned with a $500 \times 500 \times 200$ grid. The domain of the searching of the times T^I and T^{II} was specified in terms of the first natural periods in state I and state II , respectively, with a lower limit of 0.0025 times the base period and an upper limit of 0.5 times the base period. The phase ϕ of the forcing varied between 0 and 2π .

The resulting scanned space and the periodic responses can be seen in Fig. 7.

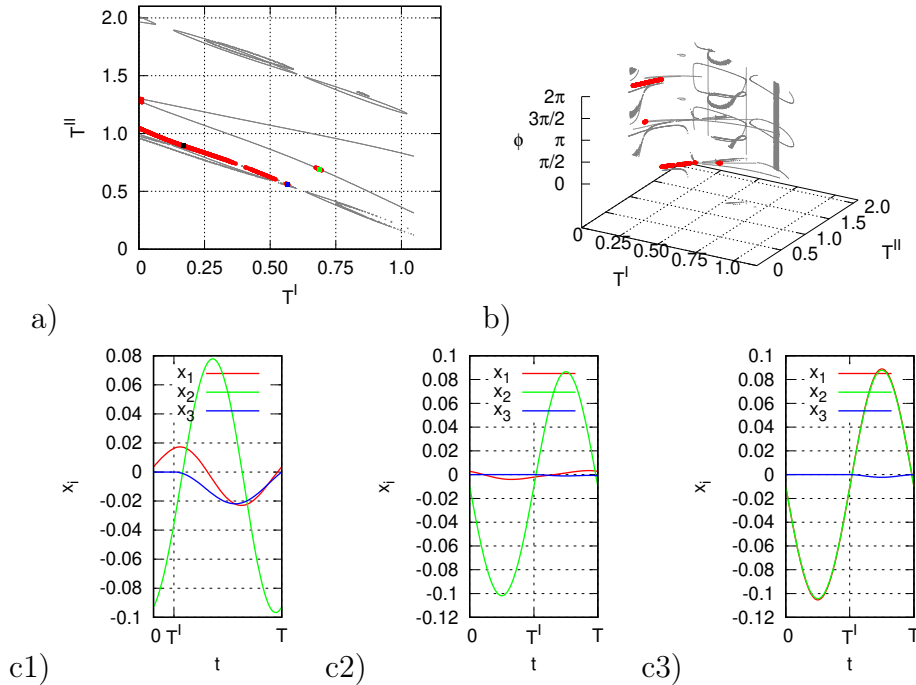


Figure 7: Solution points of the $N23$ model: periodic points with switching at the right times (gray dots), and periodic points remaining in their state and switching at the right time (with red lines) a) in the $T^I - T^{II}$ plane, b) in the three-dimensional parameter space. c1-c3) Nodal displacements of periodic responses with the periods of $T = 1.064$, $T = 1.127$ and $T = 1.340$, respectively.

Finally, the scaling of the method with the number of DOFs was analyzed. The number of DOFs was increased further until $N89$, and the runtime of the whole process was measured under the same circumstances: 4 parallel threads were used over the same domain of the GRS with the same density of grid. Figure 8 shows these data points in a diagram on a) a linear and b) a logarithmic scale. The data points are connected with a line to emphasize that the increase in the runtime in the 6 – 9 range becomes practically linear instead of a typically expected exponential growth (the slope on the logarithmic scale getting smaller).

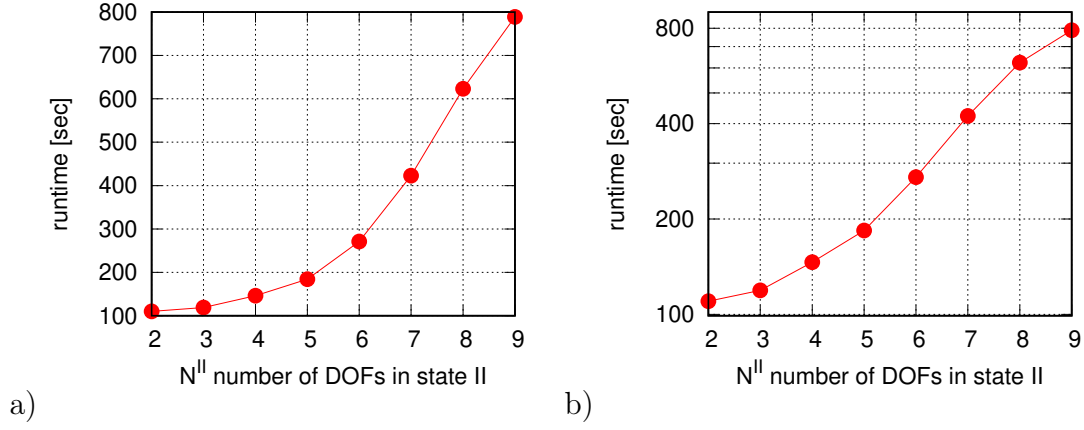


Figure 8: Scaling of the method: change of the runtime with the increase of the number of DOFs. (a) on a linear scale the increase tends to linear (b) on a logarithmic scale the curve flattens

The second example is presented here, but used in the next chapter. The $N45$ model is analyzed with forcing vectors acting only on the first mass:

$$\mathbf{q}^I = [1 \ 0 \ \dots \ 0]^\top, \quad \mathbf{q}^{II} = [1 \ 0 \ \dots \ 0 \ 0]^\top. \quad (29)$$

With a similar setting for the scanning, some of the periodic paths are shown in Fig. 9, where in b), two points were selected and shown for their periodic responses in Fig. 10

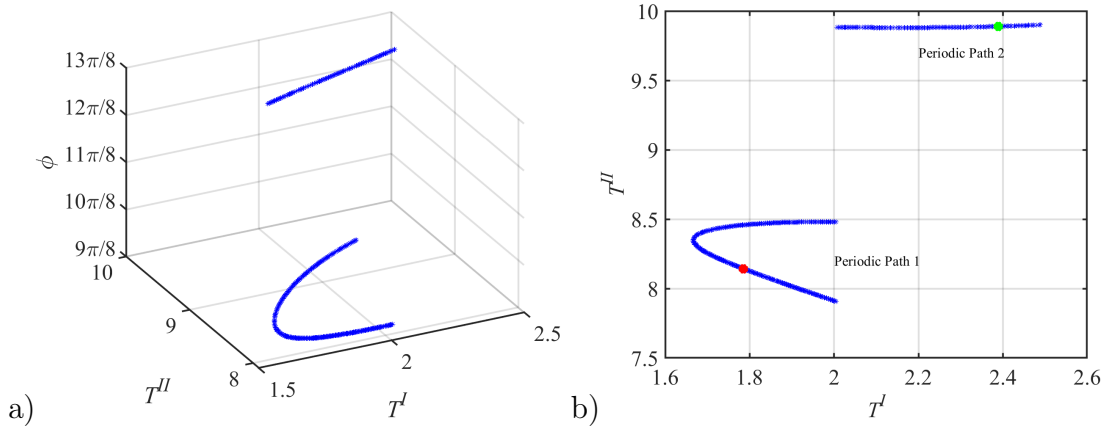


Figure 9: Solution points of the $N45$ model with the first mass forced a) in the three-dimensional parameter space b) in the $T^I - T^{II}$ plane,

4.3 Switch-free harmonic responses of the PL elastic systems

Despite the occurrence of the plastic impact in the periodic responses which divides the motion into two PL states, there still exist, under certain forcing frequencies, periodic vibrations of these systems where the system remains at the boundary of the two states; the last mass of the system has no gap with the wall and exerts no force on the wall at the same time. These vibrations are called switch-free vibrations, and the system can be treated to vibrate in any of the states for the whole period, which makes these responses of linear, harmonic characteristics. The linear nature of these vibrations allows the possibility of obtaining these solutions through analytical derivation.

For the derivation, and due to the linearity of the problem, α in Eq. (1) can be I or II . For the sake of simplicity, a forcing vector \mathbf{q}_0 that contains a unit amplitude in all its

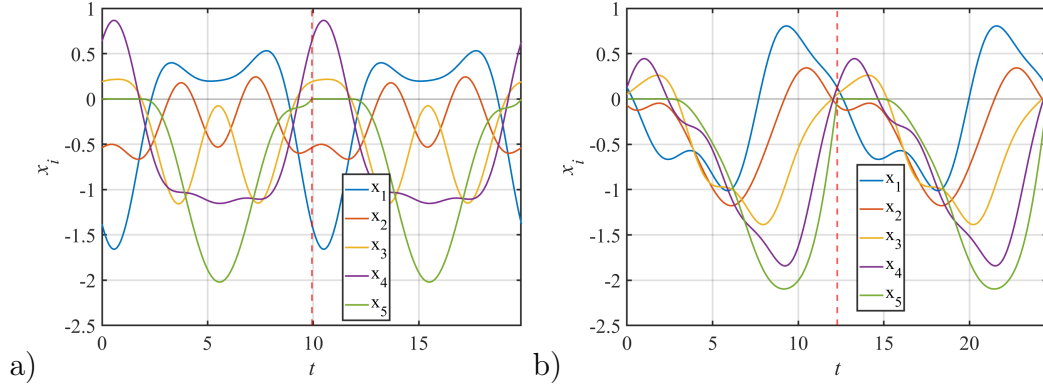


Figure 10: Nonlinear periodic responses of the system at coordinates: a) $T^I=1.7748$, $T^{II}=8.1525$, $\phi=3.5495$ (red dot) b) $T^I=2.3876$, $T^{II}=9.8894$, $\phi=4.8050$ (green dot)

entries is used. If a solution of the form $\mathbf{x}(t) = \mathbf{x}_0 \cos(\omega t)$ is searched for, the amplitude of the steady-state response to the harmonic forcing can be obtained from:

$$(\mathbf{K} - \omega^2 \mathbf{M}) \mathbf{x}_0 = \mathbf{q}_0 \quad (30)$$

with the inverse of the dynamic stiffness matrix:

$$\mathbf{x}_0 = \mathbf{K}_d^{-1} \mathbf{q}_0, \quad (31)$$

where,

$$\mathbf{K}_d = \mathbf{K} - \omega^2 \mathbf{M} \quad (32)$$

is the tridiagonal dynamic stiffness matrix, with a main diagonal of x values, where $x = 2 - \beta^2$, $\beta = \omega/\omega^*$ and $\omega^* = \sqrt{k/m}$, except the (N, N) entry is $x - 1$. The off-diagonal values are -1 . The inversion of this matrix can be performed with the help of Sherman-Morrison (SM) formula, where a matrix of an already-known inverse, let us call it A , is modified by a dyad, enhancing the computational effort for large dimensional problems on one hand, and decreasing the possibility of occurring singularities on the other hand. The solution can be simplified when using trigonometry:

$$2 \cos(\vartheta) = x. \quad (33)$$

Since we are interested in those frequencies that result in $x_{0N} = 0$, and after modifying matrix A with a dyad, the sum of the entries in the N^{th} row of matrix A is:

$$\sum_{j=1}^N \sin(j\vartheta) \left[\frac{1}{\sin((N+1)\vartheta)} + \frac{\left[\frac{\sin(N\vartheta)}{\sin((N+1)\vartheta)} \right] \frac{1}{\sin((N+1)\vartheta)}}{1 - \frac{\sin(N\vartheta)}{\sin((N+1)\vartheta)}} \right]. \quad (34)$$

The sum in Eq. (34) is zero if the sum of the quantity between the brackets is zero or:

$$\sum_{j=1}^N \sin(j\vartheta) = 0, \quad (35)$$

for which there are two groups of solutions:

$$\vartheta = \frac{2\pi r}{N}, \quad \vartheta = \frac{2\pi q}{N+1}, \quad (36)$$

where r and q are integers. Therefore, the solutions for this problem are:

$$\vartheta_j = \frac{2j + 1 - (-1)^j}{2N + 1 - (-1)^j} \pi. \quad (37)$$

Accordingly, the forcing frequencies that result in zero displacement at the N^{th} mass can be obtained from:

$$\omega_j^2 = \frac{2k}{m} (1 - \cos \vartheta_j). \quad (38)$$

Substituting ϑ from Eq. (33) in Eq. (35), the formula expands to become:

$$\sum_{j=1}^n \sin \left(j \left[\cos^{-1} \left(1 - \frac{\omega^2}{2\omega^{*2}} \right) \right] \right) = 0. \quad (39)$$

The solutions of this trigonometric constraint yield the switch-free vibration of the PL elastic system, as shown in Fig. 11

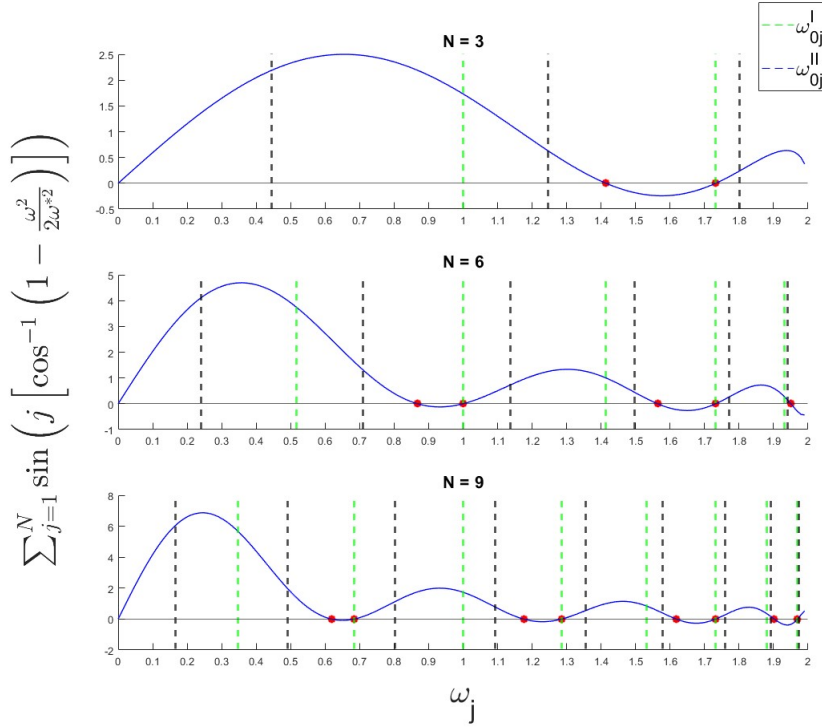


Figure 11: The trigonometric function in Eq. (39) as a function of the forcing frequency. The natural circular frequencies of the sticking (green) and free-flight (black) states are indicated as vertical dashed lines.

5 Characterization of the damping in forced piecewise linear elastic structures

In this chapter, the calculation of the energy dissipation caused by the plastic impact is presented as the difference between the kinetic energy pre- and post-impact. This energy loss is dispersed over the period of vibration of an equivalent linear system that of the PL elastic system analyzed in Chapter 4, meaning that the linear system vibrates with the same forcing frequency and phase angle as the PL elastic structure. From this

equivalence, a formula for the EVDR is derived for each of the periodic paths of the harmonically forced PL elastic structure, with an example shown of a discrete model that is forced on one single DOF. The effect of changing the position of the force on the EVDR is shown since the periodic paths, naturally, change their position almost always in the GRS as the position of the forcing changes. Finally, the effect of changing the number of DOFs in a discrete model on the EVDR is shown.

5.1 Calculation of the energy dissipation

At time instant $t = T^I + T^{II}$, the system experiences a plastic impact at the boundary, causing the N^{II} -th mass to stop and the system to switch from state II back to state I . Since the kinetic energy is directly related to the velocity, a part of it, which is associated with the motion of the N^{II} -th DOF, is lost in this incident, while the potential energy passes to the next period of vibration without any loss.

The kinetic energy of the system in state α is calculated as:

$$\mathcal{E}_K^\alpha(t) = \frac{1}{2} \sum_{j=1}^{N^\alpha} \dot{\eta}_j^{\alpha 2}(t). \quad (40)$$

Similarly, the total potential energy, originating from the stiffness matrix, is:

$$\mathcal{E}_P^\alpha(t) = \frac{1}{2} \sum_{j=1}^{N^\alpha} \omega_{0j}^{\alpha 2} \eta_j^{\alpha 2}(t). \quad (41)$$

For the same periodic solutions presented in Fig. 10, the kinetic, potential and total energies are shown in Fig. 12:

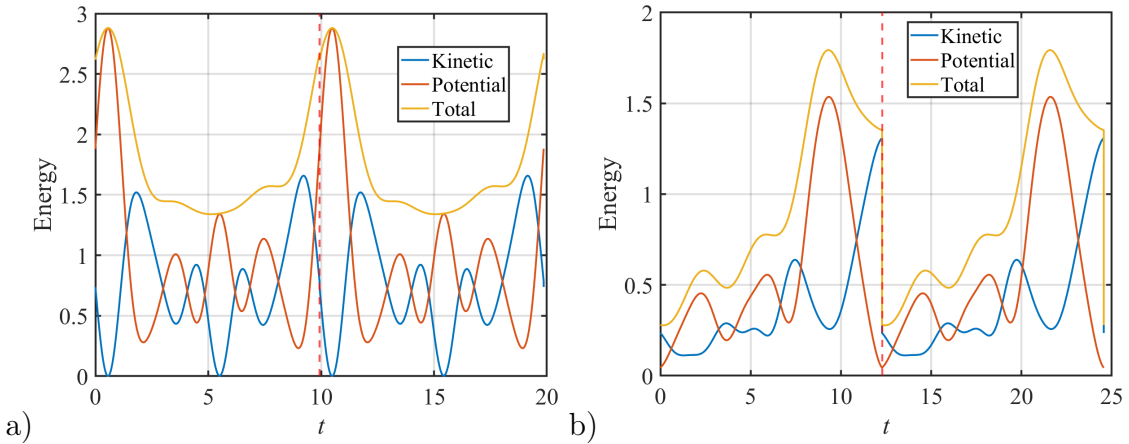


Figure 12: a) Mechanical energy of the point at the red dot in Fig. 9b) (vertical dashed line at $T = 9.9273$) occurs. b) Mechanical energy of the point at the green dot in Fig. 9b) (vertical dashed line at $T = 12.277$)

The plastic impact at $t = T$ causes an energy loss, which can be calculated from the change of the kinetic energy:

$$\Delta_{PL} = \mathcal{E}_K^{II}(T) - \mathcal{E}_K^I(T) = \frac{1}{2} \sum_{j=1}^{N^{II}} \dot{\eta}_j^{II 2}(T) - \frac{1}{2} \sum_{j=1}^{N^I} \dot{\eta}_j^{I 2}(0). \quad (42)$$

5.2 Equivalent viscous damping ratio for the forced PL elastic structure with two states

Viscous damping is widely used in mechanical and civil engineering practices due to its simplicity from a mathematical point of view, even though it does not represent the real behavior in the hysteresis diagram of dynamically loaded structures.

For a SDOF system, the energy loss due to viscous damping is the integral of the damping force times the velocity over the period of vibration:

$$E_D = \int_{T^*} 2\omega_0\xi \dot{\eta}(t) \cdot \dot{\eta}(t)dt, \quad (43)$$

where ξ is the viscous damping ratio and $\dot{\eta}$ is the modal velocity. Equation (43) can also be written as:

$$E_D = 2\omega_0\xi\Psi, \quad (44)$$

where:

$$\Psi = \int_{T^*} \dot{\eta}(t)^2 dt. \quad (45)$$

For a PL MDOF system with two states, it requires the summation of the modes to be taken for the Ψ^α functions in each state as:

$$\Delta_d = 2\xi \left(\sum_{j=1}^{N^I} \Psi_j^I \omega_{0j}^I + \sum_{j=1}^{N^{II}} \Psi_j^{II} \omega_{0j}^{II} \right). \quad (46)$$

By equating Eq. (42) to (??) and solving for ξ , the equivalent viscous damping ratio (EVDR) for a PL MDOF system with two states writes as:

$$\xi_{eq} = \frac{\Delta_{PL}}{2 \left[\sum_{j=1}^{N^I} \Psi_j^I \omega_{0j}^I + \sum_{j=1}^{N^{II}} \Psi_j^{II} \omega_{0j}^{II} \right]}. \quad (47)$$

Showing the results of Eq. (42) and (47), the energy loss at the end of the period for all the solution points in the periodic paths and the ξ_{eq} values are presented in Fig. 13.

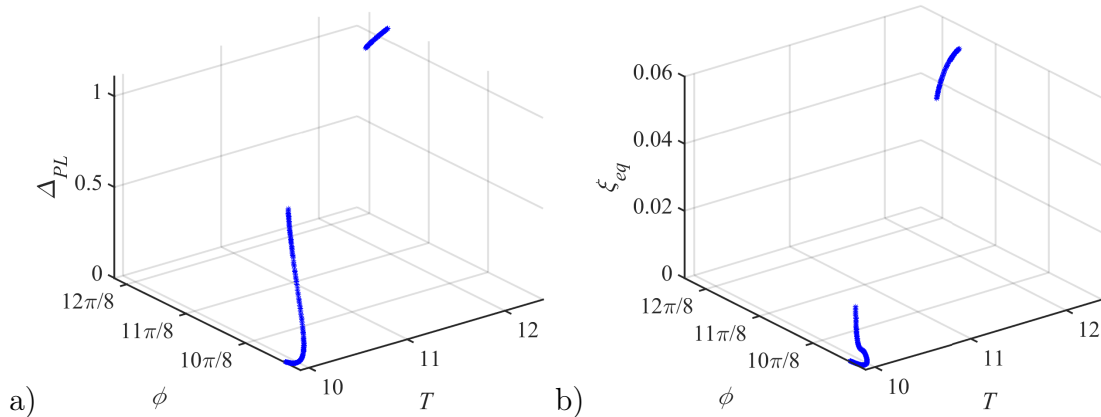


Figure 13: a) The energy loss of the PL system Δ_{PL} against the total period of forcing and the phase angle. b) Equivalent viscous damping ratio as a function of T and ϕ

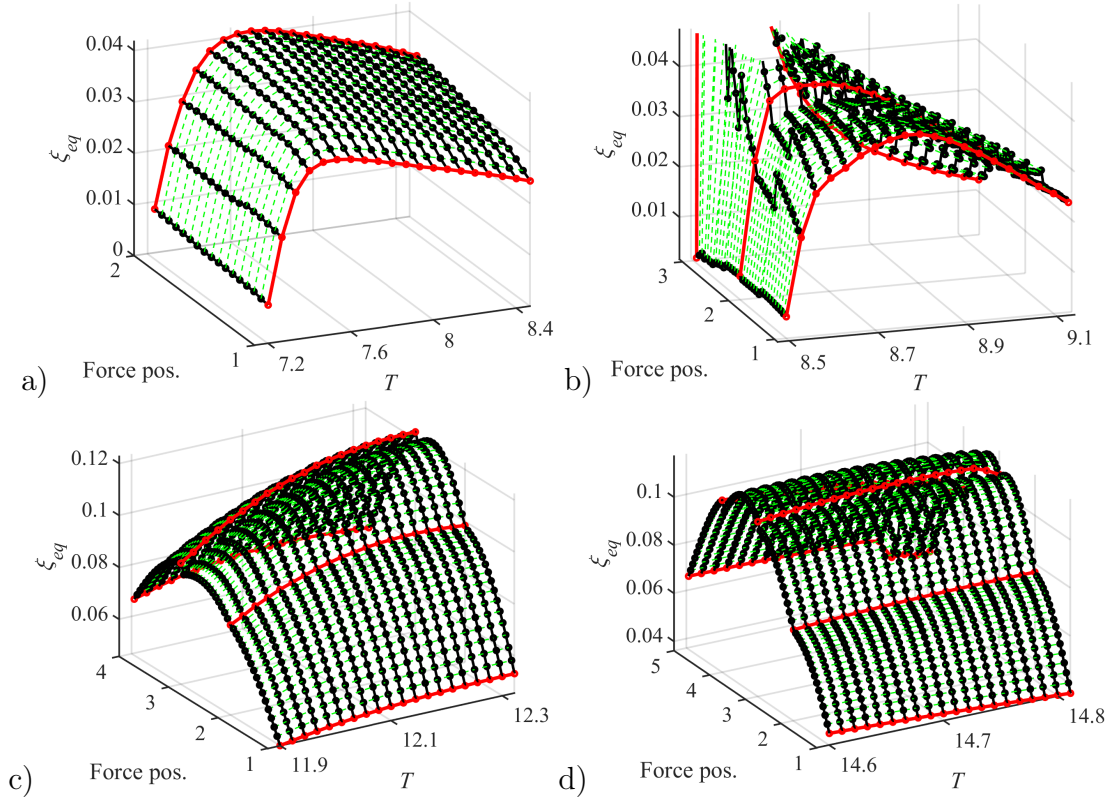


Figure 14: Equivalent viscous damping ratio with different positions of excitation force. Red dots represent modes where a single node is forced, and black dots represent modes where a combination is forced. a) $N23$, b) $N34$, c) $N45$, d) $N56$,

5.3 Effect of the loading position on ξ_{eq}

The position of the exciting force affects the values of ξ_{eq} . The forcing vector q_0 in Eq. (29) is applied in such a way that a unit force changes its place along the system, and ξ_{eq} is calculated in each case. In Fig. 14, one can see this effect, that the equivalent damping ratio increases as the position of the force moves towards the middle of the structure, and this behavior is obvious in Fig. 14c) and d).

6 New Scientific Results

6.1 Introduction

Piecewise linear elastic structures are those structures whose stiffness experiences a piecewise constant nature during vibration, depending on their topological changes. In the range where the stiffness is constant, the behaviour will be linear elastic. So, piecewise linear elasticity also means that as long as the structure maintains the same stiffness, i.e., over the same linear segment of its stress-deformation relationship, the linearity allows the application of modal analysis. Sources of piecewise linearity in nature can be the slackening of a tensioned cable and the closure of an open gap.

6.2 Thesis 1

6.2.1 Context

Slackening of a tensioned cable supporting a structure can result in piecewise linear elastic behavior. An example of that is a continuum beam supported by a block-and-tackle suspension system. This type of suspension offers a way of supporting structural elements in multiple points with a slight increase in the static indeterminacy. In this constraint, a cable is driven through pulleys placed at certain points along the beam length. The aim was to analyze the special (theoretical) case of a simply-supported beam where it is supported by a cable, and the pulleys are continuously placed along a certain segment of the beam. The source of the piecewise linearity in our beam is that under any displacement, the cable is either slacked or tensioned, which divides the motion into two piecewise linear states. In the case of a slackened cable, the beam is said to be in the passive state, while in the case of a tensioned cable, the beam is said to be in the active state. In this thesis, the study on this structure was restricted to a special case where the integral of the suspended points' displacements is equal to zero.

6.2.2 Thesis statement 1

I derived a semi-analytical approach to analyze the effect of the continuous block-and-tackle suspension on the free vibration and buckling of a simply supported single-span beam. The analysis is restricted to the case where the integral of the supported points' displacements is zero. The effect of the suspension is analyzed as a function of the length of the suspended segment. The natural circular frequencies or the critical forces of the beam are calculated as a function of the length of the continuous support and presented in a frequency map or a buckling map, respectively.

I validated my semi-analytical method against a finite element model. Modeling-wise, I substituted the block-and-tackle suspension system by a symmetrically-positioned swing system that is used for even distribution of loads in laboratory experiments. For a generic case, I constructed a series of FE models to perform convergence analyses of the mesh and the stiffness of the swing system elements.

Relevant publications: [I]

6.3 Theses 2-4

6.3.1 Context

The opening of a clearance or a possible contact interaction of a structure with its surroundings is a source of the piecewise linear elastic behaviour that can appear in the structural engineering world. An example of this type of structure is a discrete bar in tension and compression with a unilateral contact with a rigid barrier at one of its masses. This system is said to be in a free-flight state as long as there is no touch between the structure and the barrier during vibration, while it is said to be in a sticking state as long as it is in touch with it. The determination of the behaviour of the piecewise linear elastic structures is highly influenced by the characteristics of the impact happening against that barrier. A perfectly plastic impact was assumed at the gap closure between the system and the rigid barrier, meaning that the system instantaneously partially loses its kinetic energy. With these assumptions, this piecewise linear elastic structure undergoes chaotic responses even under periodic dynamic forcing, and the question here is to find a special type of periodic motions that go into one state switch in each direction.

6.3.2 Thesis statement 2

I introduced a new solution method for calculating a special group of periodic paths and vibrations for harmonically forced piecewise linear elastic structures. The method can be used for piecewise linear elastic MDOF systems with two linear states, provided that the unloaded equilibrium position of both states coincides. While the method is extendable to include more state switches per period, the desired periodic vibrations are those vibrations that perform exactly, and only, one switch in each direction during a period of forcing. The calculation is based on scanning a three-dimensional parameter space: the time spent in each piecewise linear state and the forcing phase angle. This scanning allows the finding of all solutions in the scanned region and it finds disconnected branches too. The first step of the method is to find the periodic initial conditions through a consecutive substitution of the modal phases at the state switching time instants. The second step is to scan the parameter space to find periodic solutions that fulfill the switching conditions. The third step is to filter the obtained solutions of the scanning that switch in an undesired time instant. I also analyzed the scaling of the method when changing the number of degrees-of-freedom, where the runtime of the whole scanning process for each discretization under the same circumstances was measured. I showed that the runtime varies linearly with the change of the number of degrees-of-freedom.

Relevant publications: [II]

6.3.3 Thesis statement 3

I calculated nonlinear periodic forced responses of a two-state piecewise linear elastic bar in tension and compression with different discretizations and under several loading scenarios. The first loading scenario was the support vibration, where responses close to linear characteristics were found, and other vibrations were noticed to have the mass in contact barely moving from the barrier when the gap opens, making it hard to distinguish the state of vibration. The second loading scenario was positioning one single force at different locations along the structure. Moving the load position resulted in vibrations where the amplitudes of the displacements are at their highest when the force is acting around the midpoint of the structure. I found that for some of the analyzed discrete models, the periodic paths were identical in the Global Representation Space even when changing the loading position.

Relevant publications: [II],[IV]

6.3.4 Thesis statement 4

I derived a method for obtaining the forcing frequencies that result in switch-free vibrations for a two-state piecewise linear elastic structure. The system is assumed to vibrate on the boundary of the two piecewise linear states for the whole period of forcing without a jump in the stiffness, a fact that explains the linear, harmonic nature of these motions. The derivation is based on the direct solution of the nonhomogeneous differential equation of motion of multi-degree-of-freedom systems to form the dynamic stiffness matrix. I derived a simple trigonometric constraint that can be defined for the available switch-free vibrations of different analyzed discrete models with a given forcing configuration.

Relevant publications: [III]

6.4 Thesis 5

6.4.1 Context

The piecewise linear states of stiffness that are forming in structures with contacts result from an inelastic or a perfectly plastic impact with a rigid barrier in the surroundings of the structure. This impact introduces a sudden change in the domain of the vibration, which explains the chaotic response of these structures even under harmonic forcing. For this, in Thesis 2, I developed a method for the calculation of a special type of periodic paths and responses where there happens one impact per period of forcing. The impact also introduces a partial energy loss for discrete piecewise linear elastic systems due to the sudden loss of velocity of the impacting parts with the rigid barrier. The question was to quantify the energy losses happening at the end of the period along the periodic paths in the parameter space.

6.4.2 Thesis statement 5

I derived a formula to characterize the energy dissipation caused by the purely plastic impact of two-state harmonically forced piecewise linear elastic systems. I substituted this damping with a single equivalent viscous damping ratio. The derived formula revealed a dependence on the kinetic energy of the system and the frequency ratio. I analyzed the equivalent viscous damping ratio as a function of the loading position and forcing period for a piecewise linear bar in tension and compression model with different discretizations. The equivalent damping ratio resulting from the different loading scenarios on the piecewise linear elastic systems does not appear to be significantly higher than the 10% damping ratio, which is typically used in the structural engineering practice. I concluded that it is sufficient to analyze the equivalent damping with the forcing of certain DOFs, and there is no need to check all possible combinations.

Relevant publications: [IV]

References

Gáspár, Z., G. Domokos, and I. Szeberényi (1997). “A parallel algorithm for the global computation of elastic bar structures”. In: *Computer Assisted Mechanics and Engineering Sciences* 4.1, pp. 55–68.

Own publications forming the basis of the new scientific results

- [I] Németh, R. K. and Alzubaidi, B. (2021). “The Effect of continuous suspension constraint on the free vibration and buckling of a beam.” In: **Periodica Polytechnica Civil Engineering** 65.3, pp. 977–987. DOI: 10.3311/PPci.17954.
- [II] Alzubaidi, B. and Németh, R. K. (2023). “Modal analysis-based calculation of periodic nonlinear responses of harmonically forced piecewise linear elastic systems.” In: **Journal of Sound and Vibration** 549, p. 117576. ISSN: 0022-460X. DOI: 10.1016/j.jsv.2023.117576.
- [III] Alzubaidi, B. (2024). “Switch-free harmonic vibrations of multi-degree-of-freedom piecewise linear elastic structures.” In: Proceedings of the 15th PhD Symposium, Budapest, Hungary. **International Federation for Structural Concrete (fib)**, pp. 333–340.
- [IV] Alzubaidi, B. and Németh, R. K. (2025). “Characterization method of the damping in harmonically forced two-state piecewise linear elastic structures.” In: **Computer Assisted Methods in Engineering and Science**. Manuscript accepted for publication.